New Developments in Planar Array Infrared Spectroscopy

ISABELLE PELLETIER, CHRISTIAN PELLERIN,* D. BRUCE CHASE, and JOHN F. RABOLT†

Department of Materials Science and Engineering, University of Delaware, Newark, Delaware 19716 (I.P., C.P., J.F.R.); and Central Research and Development, DuPont Experimental Station, Wilmington, Delaware 19880 (D.B.C.)

A planar array infrared (PA-IR) spectrograph offers several advantages over other infrared approaches, including high acquisition rate and sensitivity. However, it suffers from some important drawbacks, such as a limited spectral range and a significant curvature of the recorded spectral images, which still need to be addressed. In this article, we present new developments in PA-IR spectroscopy that overcome these drawbacks. First, a data processing method for the correction of the curvature observed in the spectral images has been developed and refined. In addition, a dual-beam instrument that allows the simultaneous recording of two independent spectral images has been developed. These two improvements have been combined to demonstrate the real-time background correction capability of PA-IR instruments. Finally, the accessible spectral range of the PA-IR spectrograph has been extended to cover simultaneously the methylene stretching (3200–2800 cm^{-1}) and the fingerprint (2000–1000 cm^{-1}) spectral regions.

Index Headings: **Planar array infrared spectroscopy; Dual-beam accessory; Real-time background correction.**

INTRODUCTION

During the last fifteen years, a growing number of large, relatively inexpensive, and high-quality infrared linear array and focal plane array (FPA) detectors have become commercially available. While these detectors are increasingly popular for use in Fourier transform infrared (FT-IR) imaging systems[1–6] to map the spatial distribution of chemical species in matrices such as living tissues[2,7–11] and polymeric systems,[12–17] they have also found uses in dispersive infrared instruments. For example, in 1990, Richardson et al. described a prototype dispersive infrared spectrometer using a 32-element linear InSb array detector.[18,19] They reported that this instrument could measure infrared spectra in the 2400–2650 cm^{-1} region in 4 μs, with a nominal resolution of 32 cm^{-1} and a root mean square (rms) noise level of ~0.01 absorbance units (A.U.). Hamm et al.[20] and Arrivo et al.[21] used a mercury cadmium telluride (MCT) linear array detector and an InSb FPA detector to record infrared spectra having spectral ranges of 65 and 400 cm^{-1} with resolutions of 3 to 10 cm^{-1} and 15 cm^{-1} and rms noises of 4×10^{-5} and 3×10^{-4} A.U., respectively. In 2002, Elmore et al. reported the construction of a dispersive infrared spectrograph using a continuous broadband source and a 320 × 256 InSb FPA detector.[22] This planar array infrared (PA-IR) spectrograph could record spectra in the 3400–2000 cm^{-1} region with a resolution of 8 cm^{-1} and a peak-to-peak noise of $\sim 1 \times 10^{-3}$ A.U. for an integration time of 1.5 ms. More recently, Pellerin et al. presented a new PA-IR instrument using a 256 × 256 MCT focal plane array that was capable of recording infrared spectra in the 2000–975 cm^{-1} region with a resolution between 7 and 14 cm^{-1} and a peak-to-peak noise as low of 2.4×10^{-4} A.U.[23]

Planar array infrared spectroscopy provides a number of options and advantages over conventional dispersive and FT-IR spectrometers. First, the use of a large FPA detector eliminates the need for an exit slit and provides a true multichannel advantage comparable to the multiplex advantage of an interferometer. Second, the fast response of the InSb and MCT FPAs leads to short integration times that allow time-resolved spectroscopic measurements to be carried out. Furthermore, the large number of rows in the FPA detectors enables pixel binning in order to increase the signal-to-noise ratio of the spectra and allows the simultaneous detection of two separate and independent spectral images. The latter feature has been used to simultaneously record orthogonally polarized spectra during the electric-field-induced reorientation of liquid crystals.[23] In addition, it has also been demonstrated that PA-IR spectroscopy could be used to record simultaneously the sample and background spectra on different portions of the FPA, thus enabling a real-time background correction.[22] Finally, PA-IR spectrographs are rugged and well suited for portable and compact configurations because there are no moving parts during data acquisition.

Despite all these advantages, PA-IR instruments still have limitations. First, their spectral range is a function of the dispersion of the grating employed and is currently limited to a width of ~600 cm^{-1}. Secondly, pixel binning and real-time background correction are not easy to perform because of the curvature of the images recorded by the FPA detector. Such curvature, which has been attributed to both the out-of-plane diffraction by the grating and to the use of off-axis mirrors,[24] is an important issue because the rows of a curved spectral image cannot be binned without sacrificing spectral resolution. Similarly, the real-time background correction will introduce severe artifacts if the initial image is curved because any given spectral element in the sample part of the image will be shifted with respect to that in the background part of the same image. Various attempts have been made to deal with image curvature, including the use of a curved entrance slit,[24,25] symmetrically curved entrance and exit slits on an Ebert monochromator,[26–28] convex spherical gratings,[29] and off-axis compensating entrance optics.[30] Unfortunately, these approaches are not very general and hence are not easily transferable for use with a PA-IR spectrograph.

Received 25 September 2004; accepted 5 November 2004.

* Address as of 1 February 2005; Département de Chimie, Université de Montréal, Montréal, Québec, Canada.

† Author to whom correspondence should be sent. E-mail: rabolt@udel.edu.

0003-7028/05/5902-0156$2.00/0

In this paper, several recent developments in planar array infrared spectroscopy are discussed. First, a dual-beam PA-IR spectrograph that allows the simultaneous recording of two independent spectral images will be described. Second, a new data processing method for the correction of the curvature observed in the spectral images recorded by the FPA detector is described. These two developments were combined and the first demonstration of real-time background correction using a PA-IR spectrograph was obtained. Finally, by using concurrently two different diffraction gratings, the accessible spectral range of the PA-IR spectrograph has been extended to cover simultaneously the methylene stretching (3200–2800 cm^{-1}) and the fingerprint (2000–1000 cm^{-1}) spectral regions.

EXPERIMENTAL

Planar Array Infrared Spectrograph. The instrument used in this work was based on that described by Pellerin et al.[23] In this spectrograph shown in Fig. 1A, the light emitted by a broadband infrared source was collected and collimated by an off-axis parabolic mirror (M1). For single beam measurements, this collimated beam was directly focused on the entrance slit by a spherical mirror (M2), while it passed through the dual-beam accessory described in the next section for the multiple-beam experiments. After the slit, the infrared beam was collimated by another spherical mirror (M3) and projected on a plane-ruled diffraction grating with either 50, 75, 150, or 300 grooves/mm (SPEX, Edison, NJ). Finally, a spherical mirror (M4) and a Ninox multi-element lens (Janos Technology, Townshend, VT) was used to collect and focus the light beam onto the focal plane of a 256 $\times$ 256 MCT FPA with 40 $\times$ 40 μm pixels (Santa Barbara Focalplane, Goleta, CA).

Dual Beam Accessory. Figure 1B contains a schematic diagram of the dual-beam accessory that was introduced in the collimated beam between mirrors M1 and M2 for the multiple-beam experiments. The incoming light beam was first split in two parts by two plane mirrors (A) with their edges cut at 45° and assembled to form a 90° angle. Spherical mirrors (B) were then used to focus the beams through the top and bottom sample holders (C). Next, the beams were collected by another set of matched spherical mirrors (D) and recombined using two other plane mirrors assembled at 90° (E). These mirrors reflected the collimated beams toward the M2 mirror of the PA-IR spectrograph. The dual-beam accessory can be used for the simultaneous recording of two samples or that of a sample and its background, as shown in Fig. 1C. In this figure, the top portion shows the strong absorption bands (dark curved vertical lines) of a polystyrene sample while the bottom portion only shows the weak and narrow absorption bands of water vapor in the reference beam.

Recording and Processing of Spectral Images. The spectral images were recorded using the WinIR 3.6.0.5 software (Santa Barbara Focalplane, Goleta, CA) and subsequently processed with home-written programs in MatLab 5.3 (MathWorks, Natick, MA). A reference image ($I_{reference}$) was recorded with an open optical path before recording the spectral image of the sample (I_{sample}). In addition, dark background images were collected before or after recording the sample and reference images ($I_{dbk\ sample}$ and $I_{dbk\ reference}$). These dark background images were obtained with the optical path blocked by a room-temperature anodized metal plate in order to compensate both for the thermal contribution of the environment to the FPA response and for any potential stray light reaching the detector. For a given sample, an absorbance image (A) was calculated using the following equation:

$$A = -\log_{10}\left(\frac{I_{sample} - I_{dbk\ sample}}{I_{reference} - I_{dbk\ reference}}\right) \quad (1)$$

To obtain a spectrum with maximum signal-to-noise ratio, the rows of the absorbance image were binned. When the dual-beam accessory was used, the top and bottom portions of the absorbance image were binned separately, thus yielding two spectra. The spectrum obtained from the background section of the absorbance image was then subtracted from that of the sample section of the same image in order to obtain the final spectrum. When appropriate, the pixel number scale of some of the spectra presented in this article were converted to a wavenumber scale using the procedure described by Pellerin et al.[23]

Correction of Image Curvature. As can be seen in Fig. 2A, the images recorded by the FPA detector, and thus the absorbance images calculated using Eq. 1, are curved. To avoid a significant loss of resolution upon row binning, the absorbance images were corrected according to the following three-part procedure prior to binning. In the first step, the spectral image of a uniform sample placed in front of the slit and having multiple absorption bands throughout the spectral range of interest was recorded. For this purpose, a 38 μm thick polystyrene (PS) film was used. A home-written MatLab program was then used to calculate the absorbance image of this sample (using Eq. 1) and to determine which rows of this image contained a meaningful spectrum and therefore should be used for binning. To do so, the point-by-point differences between a ''reference'' row (usually located at the center of the illuminated portion of the image) and all the other rows of the image were calculated, squared, and summed. The rows containing a spectrum (i.e., the rows similar to the reference row) had a very small sum of the squared differences (SSD) while the rows containing only noise had a very large SSD. The rows having an SSD larger than a predetermined value were excluded from the calculations while the other rows were kept for curvature correction and binning. To facilitate the next steps, the PS absorbance image was linearly interpolated by a factor of 5, leading to an image containing 1276 columns rather than 256.

In the second step of the procedure, the centers of gravity of the polystyrene bands were calculated for each of the rows kept during the first step of the procedure. Since the spectral image is curved, the centers of gravity of the different bands were located at slightly different pixel positions for each row. The centers of gravity found for the reference row were then plotted against those found for every other row and fitted using an appropriate analytical expression (linear, quadratic, or polynomial of order three or four). The fitting parameters and the SSD values calculated for each row were finally saved for use

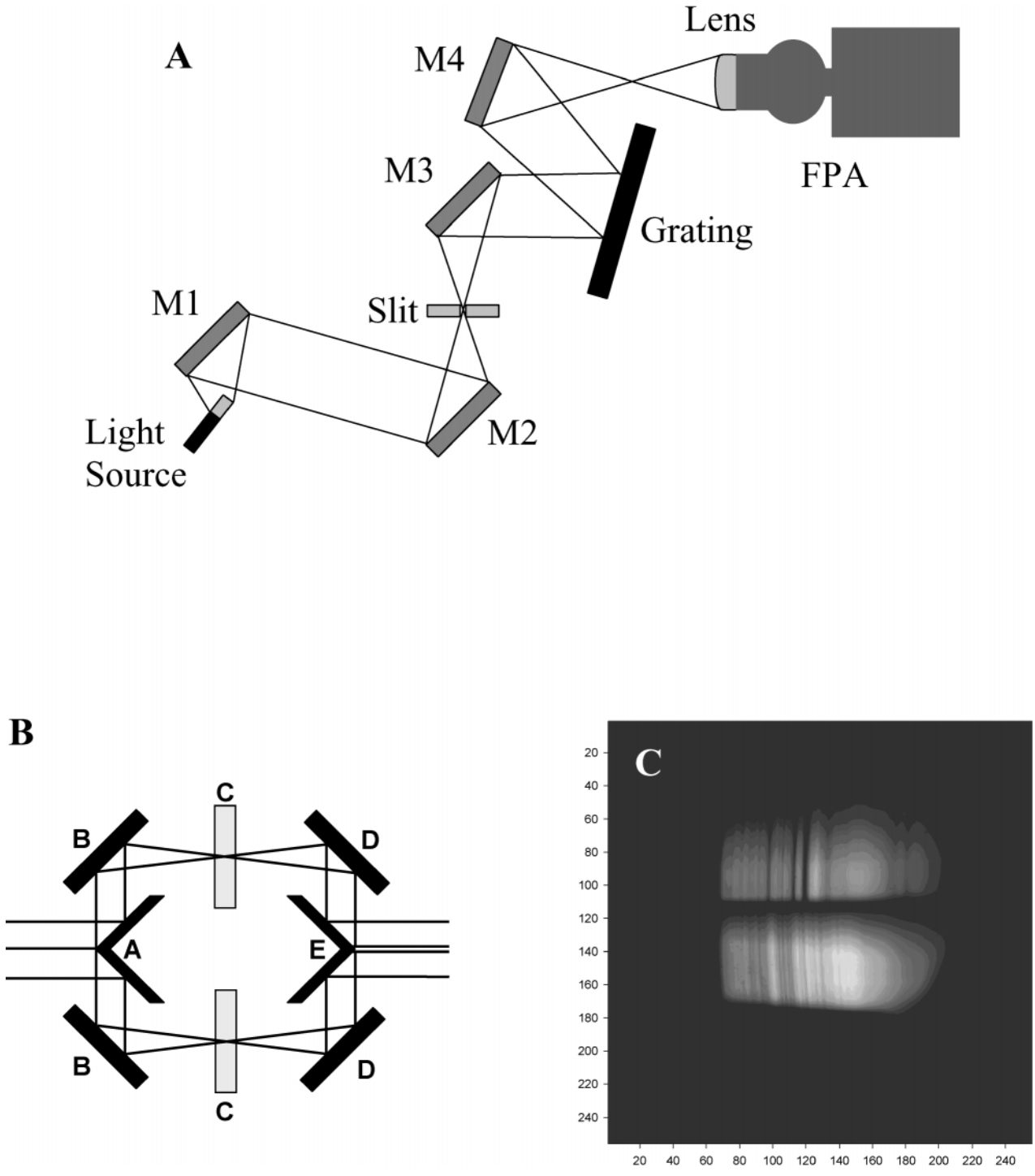

FIG. 1. (**A**) Scheme of the PA-IR spectrograph. (**B**) Scheme of the dual-beam accessory. (**C**) Spectral image recorded with a polystyrene film placed in the top portion of this accessory and air in the bottom portion. On this image, bright areas represent high single beam intensity regions.

in the final part of the curvature correction process. It should be noted that these first two steps needed to be performed only once, as the parameters thus obtained are valid for all other images recorded under the same experimental conditions.

The last part of the correction procedure uses the parameters obtained in the first two steps for the PS spectral image to correct the images of any sample recorded in the same experimental conditions as the PS image. First, the absorbance image of the sample was calculated using Eq. 1 and linearly interpolated by a factor of 5. The SSD calculated in the first step of the correction procedure were used to exclude from this image any row not containing a meaningful spectrum (the same rows that, previously, did not contain a PS spectrum). The fitting parameters determined in the second step were then used to modify the pixel numbers of every row. The result of this row-by-row pixel shift is a straightened absorbance image of the sample in which the centers of gravity of the different bands are exactly at the same pixel position

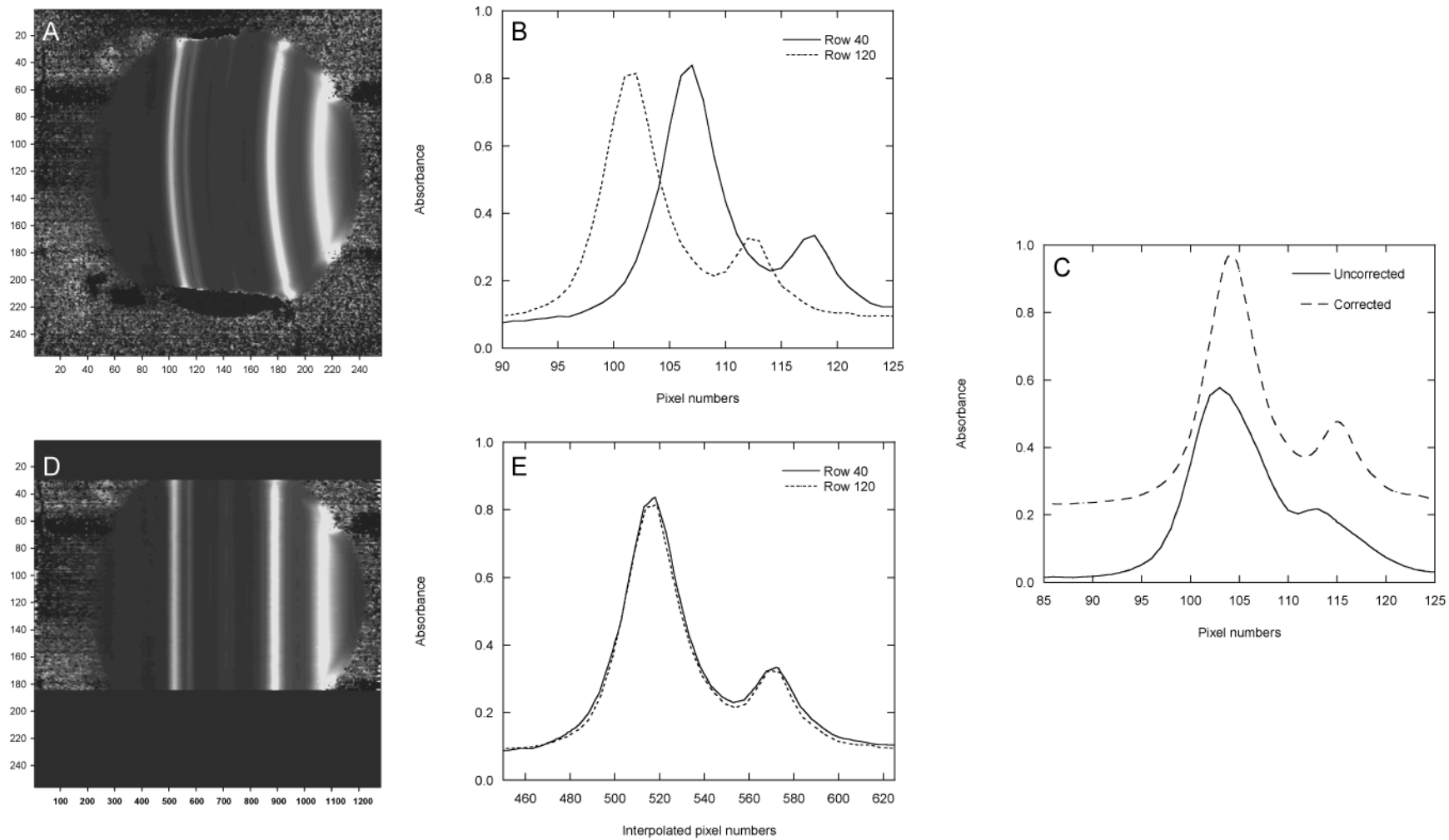

FIG. 2. Absorbance image of a polystyrene film and spectra obtained from different rows of this image for (**A** and **B**) an uncorrected image, and (**D** and **E**) a curvature-corrected image. (**C**) Average absorbance spectra obtained by binning rows from A and D. On these images, bright areas represent high absorbance regions.

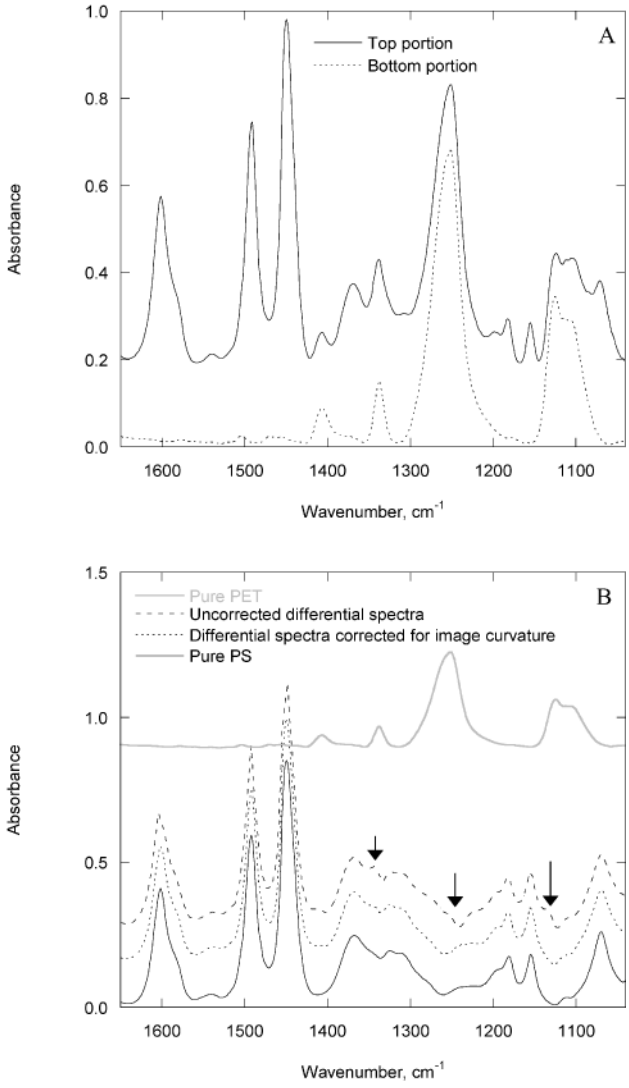

FIG. 3. (**A**) Binned absorbance spectra arising from the top and bottom parts of a spectral image recorded with a polystyrene (PS) film placed in the top portion of the dual-beam accessory and a poly(ethylene terephthalate) (PET) film placed in front of the slit of the spectrograph. (**B**) Absorbance spectra of pure PS and PET, and differential spectra (top (PS/PET) portion minus bottom (PET) portion) arising from curvature-corrected and uncorrected spectral images. The arrows point to artifacts created in the differential spectrum by the spectral subtraction.

for each row. However, because each row of this image possessed its own set of interpolated pixel numbers, direct averaging was impossible. To allow binning, each row was re-interpolated using a cubic spline function. This interpolation resulted in a straightened image in which every row had the same set of pixel numbers.

Fourier Transform Infrared Spectrometer. Fourier transform infrared spectra were collected at 4, 8, and 16 cm^{-1} resolution without zero-filling using a Nexus 670 FT-IR (Thermo Nicolet, Madison, WI) equipped with a MCT detector.

RESULTS AND DISCUSSION

Image Curvature Correction. Figure 2A shows the absorbance image of a polystyrene film, recorded in the single beam mode, before applying the curvature correction procedure. On this image, the white and light gray areas represent high absorbance regions (absorption bands) while the darker areas are due to low absorbance regions. The obvious curvature observed in this image causes the bands to appear at different pixel numbers for different rows. For example, the spectra of rows #40 and #120 have been plotted in Fig. 2B for a small spectral range. The bands in these spectra have been attributed to the ν_{9B} (strong) and ν_{9A} (weak) aromatic deformations observed at 1602 and 1585 cm^{-1}, respectively.[31] It is clear that, for this particular spectral range, the polystyrene spectrum from row #40 is shifted to the right by approximately 5 pixels with respect to that of row #120. If row binning is performed on this uncorrected image, the spectral resolution of the resulting average spectrum, shown in Fig. 2C (solid line), is much lower than that of the individual rows of the original image. In fact, comparison with FT-IR measurements (not shown) indicate that spectra extracted from individual rows possess a spectral resolution of 6 cm^{-1}, while the average spectrum obtained by row binning without correcting for the curvature possesses a resolution of only 11 cm^{-1}.

Figure 2D was obtained by applying the curvature correction procedure described in the Experimental section to the image shown in Fig. 2A. It is clear that the pixel shifting procedure has totally removed the curvature observed in the original spectral image. It should be noted that the larger number of pixel values (1276 vs. 256) on this image is due to the linear interpolation (by a factor 5) performed during the curvature correction procedure. The black regions at the top and bottom of this image are rows that have been excluded from the calculations because they possessed a large SSD and, thus, did not contain a significant spectrum. In this specific case, the rows were chosen by using row #160 as the reference row, calculating the SSD of each row between pixels 90 and 200, and keeping solely the rows having an SSD lower than 8.

The limits between which the SSD are calculated have a profound influence on the rest of the correction procedure. For example, in the present case, these limits did not include the intense band located between pixel #200 and #230. This was done in order to include in the corrected image rows 30 to 70 and 170 to 182, which do not contain this band. The reason why this band does not show up in the top and bottom portions of the image is the overfilling of the collection spherical mirror (M4) used to focus the diffracted beam onto the FPA. The round shape of the mirror can actually be distinguished in both Figs. 2A and 2D. The use of a mirror with a larger diameter would have enabled us to observe this particular band, as well as those below pixel 80, along the full height of the image. Obviously, because the band located around pixel #210 is not present in all the rows kept for the calculation, it could not be used for the fit of the centers of gravity. A linear fit was thus performed using the centers of gravity of the bands in the 85–110, 130–150 (too weak to be observed on the selected intensity scale), and 160–190 pixel ranges. Although this fit was optimized for the 85–190 pixel range (about 1650 to 1475 cm^{-1}), it appears to have nevertheless straightened, rather well, the band around pixel #210. Alternatively, an even better straightening of this band would have been possible if the image had been corrected by including the

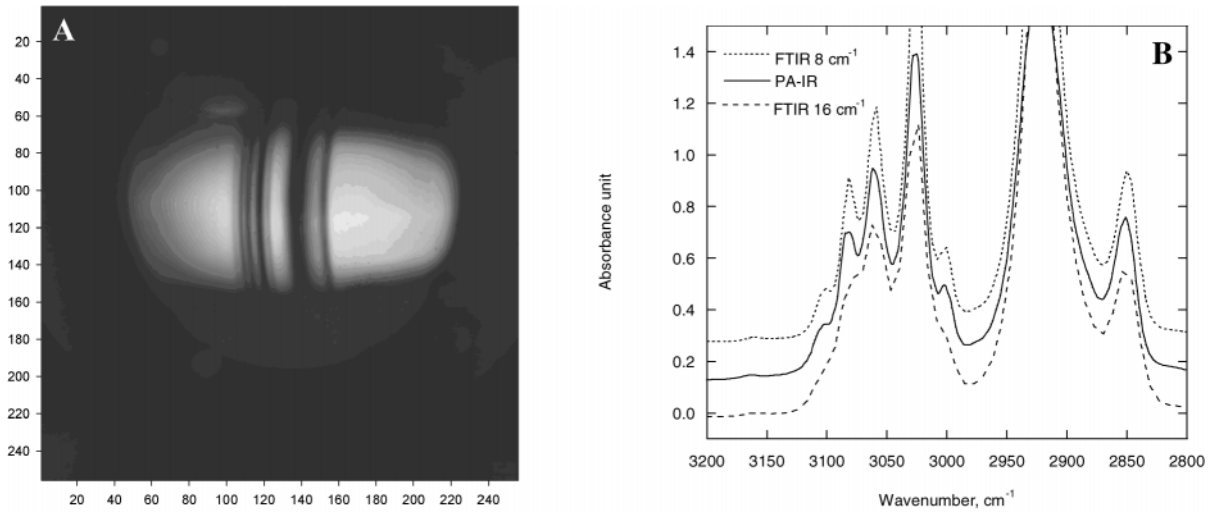

FIG. 4. (**A**) Raw spectral image of a polystyrene film in the methylene stretching spectral region. (**B**) Comparison of the binned PA-IR absorbance spectrum with FT-IR spectra recorded with spectral resolutions of 8 and 16 cm^{-1}.

center of gravity of this band along with the others. This would have preserved the entire accessible spectral range, at the expense of a reduced number of rows (101 vs. 153 rows) to average in the binning process.

Figure 2E shows the spectra obtained from rows #40 and #120 of the corrected image in the same spectral range as in Fig. 2B. In this figure, the centers of gravity of both bands are clearly located at the same position for both rows, in marked contrast to the situation before the pixel shift (Fig. 2B). This is also true for every band located in the fit optimization range and for every row kept by the correction procedure. When row binning is performed on the corrected image, the resulting spectrum (Fig. 2C, dashed line) is smoother and has a better signal-to-noise ratio than any individual row from the original image. Most importantly, this spectrum possesses exactly the same spectral resolution, 6 cm^{-1}, as that of any individual row from the initial absorbance image.

Real-Time Background Correction. Although almost all FT-IR instruments are either purged or kept under vacuum, a problem frequently encountered when performing infrared spectroscopy with single beam instruments is the imperfect compensation of the water vapor and carbon dioxide bands in the spectra. While this may not be a major issue for strongly absorbing samples, small changes in the concentration of those interfering species between the successive recording of the background and sample spectra can lead to important positive or negative spectral features when studying weakly absorbing systems such as monolayers or dilute gases. In other instances it may simply be impossible to control the environment in which the measurement is performed, for example, on-line monitoring or field applications. As discussed in the Experimental section, the use of a dual-beam accessory and a focal plane array makes possible the simultaneous recording of sample and background spectra, thus allowing the real-time background correction of the sample spectrum. If the amount of water vapor (or any other species) changes between the recording of the reference and sample spectra, the absorbance spectrum recorded in the open path part of the dual-beam accessory can be subtracted from that recorded in the part where the sample is located, resulting in the removal of the water vapor bands from the difference spectrum and thus eliminating the need for a purge.

To demonstrate the possibility of real-time background correction, a 4 μm thick poly(ethylene terephthalate) (PET) film has been introduced in front of the slit between the recording of an image of a polystyrene film placed in the top part of the dual-beam accessory and the recording of a reference image with the two beams opened. In this case, the PET film acts as an extreme case of environmental variation between the collection of the reference and sample spectra. The resulting spectral images were similar to Fig. 1C and have been corrected for the curvature in the 1850–1000 cm^{-1} spectral range using the procedure described in the Experimental section.

The binned absorbance spectra recorded in the top and bottom portions of the image are shown in Fig. 3A. The bottom portion spectrum (dotted line) shows bands due to the PET film placed in front on the slit, while the top portion spectrum (solid line) shows bands due to both the PS and PET films. In principle, the PET bands should be completely removed from the polystyrene spectrum by subtracting the spectrum obtained for the bottom part of the dual-beam accessory from that obtained in the top part. Figure 3B shows the spectra resulting from that subtraction for the curvature corrected (dotted line) and uncorrected (dashed line) images. For comparison, the spectra of pure PS (solid line) and PET (thick gray line) films are also shown in this figure. The difference spectrum obtained from the uncorrected image contains several artifacts, indicated by black arrows, located approximately at 1335, 1245, and 1135 cm^{-1}. The position of these artifacts matches that of the PET bands, indicating that they arise from the imperfect subtraction of the PET spectrum from the PS/PET composite spectrum.

In contrast, the PET spectrum was almost perfectly subtracted from the PS/PET spectrum when the curvature of the absorbance image was corrected before binning. Obviously, the curvature correction caused the PET bands to be exactly at the same position in the top and bottom sections of the image, thus enabling a very good subtraction of the PET spectrum. This result shows un-

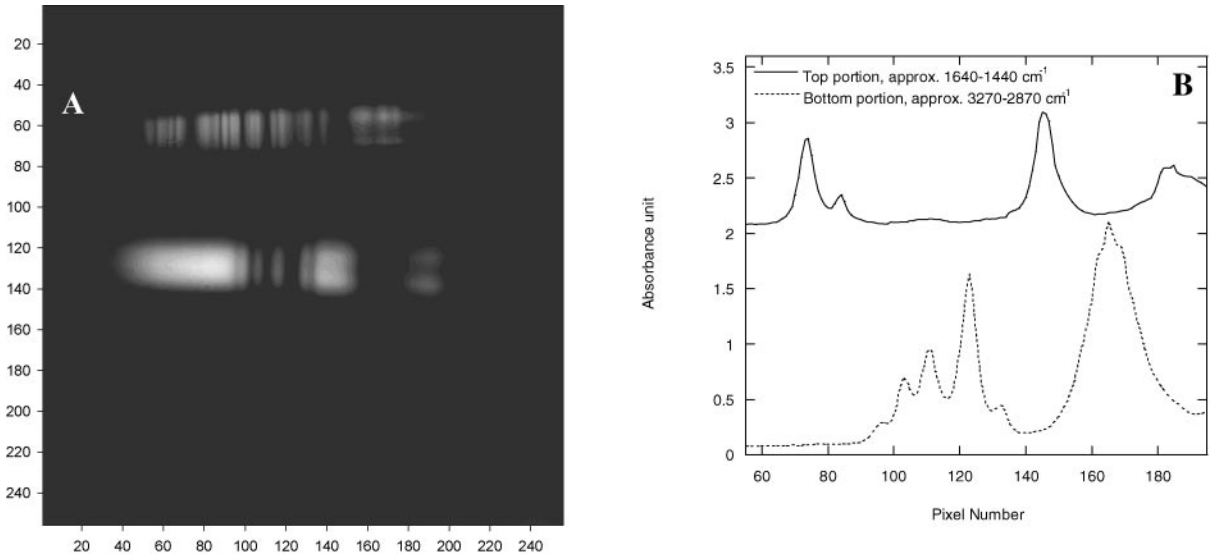

FIG. 5. (**A**) Raw spectral image of a polystyrene film recorded in the fingerprint region (top section) and in the methylene stretching region (bottom section). (**B**) Absorbance spectra obtained from individual rows located in the top and bottom sections of (A).

ambiguously that the combination of the dual-beam accessory and image curvature correction procedure allows the easy and almost complete removal of random environmental contributions from any sample spectrum. In addition to eliminating the requirement for a purged environment, this approach reduces the sensitivity of the measurements to instrumental drifts that can affect the accuracy of the measurements, for example a variation of the source intensity between the two measurements.

A drawback of the real-time background correction scheme is an increased noise level in the spectrum as compared to one recorded in the single beam mode with an identical acquisition time. A close examination of the difference spectrum obtained from the curvature-corrected image reveals that it is noisier than the polystyrene spectrum. This is simply due to the fact that the number of rows that can be binned is reduced in the dual-beam measurement as compared to the single beam case. This approach could thus prove very useful for measurements that are not noise-limited but that could suffer from significant environmental changes between the collection of the reference and sample spectra. Of course, it is always possible to increase the acquisition time (for example from 1 s to 1 min) to increase the signal-to-noise ratio.

Extension of the Spectral Range. One of the limitations of the PA-IR spectrographs described by Elmore et al.[22] and by Pellerin et al.[23] was their limited accessible spectral range, 3400–2000 cm^{-1} and 2000–975 cm^{-1}, respectively. While the spectral range of the first instrument was intrinsically limited by the response window of the InSb FPA, the MCT FPA used in the latter work can detect the radiation across the entire mid-infrared range from 4000 to 950 cm^{-1}. Figure 4A shows that, by using a 300 grooves/mm grating blazed at 4 μm and optical elements with appropriate transmission windows, it is possible to record the spectral image of a PS film in the methylene stretching region (3200 to 2800 cm^{-1}). The spectrum obtained after binning the curvature-corrected absorbance image is shown in Fig. 4B, along with the spectra of the same film recorded with an FT-IR instrument at resolutions of 8 and 16 cm^{-1}. By comparing these three spectra, the resolution of the PA-IR spectrum can be estimated to be about 12.5 cm^{-1}. It is important to note that the curvature correction and row binning produced a spectrum that is much smoother than the FT-IR spectrum recorded at a resolution of 8 cm^{-1}, even though its resolution is smaller. This indicates that the size of the detecting elements of the FPA is not the limiting factor for these spectra in determining the resolution of the spectrograph. This is due in part to the use of a slit width larger than the pixel size and is also due to imperfect optical alignment.

It should be pointed out that although the whole mid-infrared range is accessible using this instrument, it does not generate a full IR spectrum like an FT-IR does. The spectral range of a single no-moving-part PA-IR measurement is still limited to approximately 700 cm^{-1}, with the possibility of easily rotating the grating to cover a different spectral range. While this is sufficient for most studies, the possibility of recording full spectra in a single measurement would certainly eliminate one of the most important drawbacks of PA-IR vs. FT-IR spectroscopy. Figure 5A shows our first attempts towards achieving that goal. In this experiment, a mosaic grating composed of two stacked plane-ruled gratings with 300 and 75 grooves/mm was used instead of a single diffractive element. The gratings were positioned in such a way that the bottom and top portions of the image of a PS film contain spectra in the methylene stretching and fingerprint regions, respectively. This is the *first* time that a PA-IR spectrograph is shown to allow recording spectral images in those two regions simultaneously. The 75 grooves/mm grating was used in the second diffraction order, and separate order-sorting filters were used for the two parts of the image in order to preserve the photometric accuracy. Figure 5B shows individual rows from the top and bottom portion of the image in Fig. 5A. The spectral resolution of these two spectra is very similar to those observed in Fig. 4A for the methylene stretching region and in Fig. 2C for the fingerprint region.

Mosaic gratings have been used for a number of years in charge-coupled device (CCD) camera-based instruments, including Raman spectrographs, to cover two spectral ranges simultaneously. In such instruments, the use of a 1024-pixel-wide CCD camera allows coverage of the 50 to 3500 cm^{-1} Raman shift range in a single measurement with good spectral resolution. Although infrared FPAs of such width have been produced, they are not readily available to the scientific community. However, one can predict that when such detectors become available at low cost, the mosaic grating approach demonstrated in Fig. 5A will allow the measurement of a full mid-infrared spectrum using a PA-IR spectrograph in a no-moving-part single measurement. Such PA-IR instrument would still benefit from the rapid acquisition speed in the low ms range typical of these no-moving-part spectrographs. Until such FPAs are available, the use of a mosaic grating remains pertinent for applications in which the simultaneous acquisition of spectra in two limited spectral ranges is useful.

CONCLUSION

A new image curvature correction procedure has been shown to allow the binning of rows coming from an initially curved spectral image without loss of resolution. A dual-beam accessory enabling the simultaneous recording of sample and background spectra has also been developed. Together, the correction procedure and dual-beam accessory allow the real-time background correction of environmental contributions from any sample spectrum and eliminates the need for a purge. The spectral range of the PA-IR spectrograph has been extended to cover the full mid-infrared (4000–950 cm^{-1}). Moreover, spectra in the methylene stretching spectral region and in the fingerprint region have been recorded simultaneously for the first time with a PA-IR instrument. With these new developments, important drawbacks of PA-IR spectroscopy have been overcome, thus making it a serious alternative to FT-IR spectroscopy.

ACKNOWLEDGMENTS

The authors acknowledge NSF Division of Materials Research, NSF Approaches to Combat Terrorism, and NIH for partial support during the course of this work. I.P. and C.P. also thank NSERC of Canada for postdoctoral fellowships.

1. E. N. Lewis, P. J. Treado, R. C. Reeder, G. M. Story, A. E. Dowrey, C. Marcott, and I. W. Levin, Anal. Chem. **67,** 3377 (1995).
2. E. N. Lewis, A. M. Gorbach, C. Marcott, and I. W. Levin, Appl. Spectrosc. **50,** 263 (1996).
3. E. N. Lewis, L. H. Kidder, J. F. Arens, M. C. Peck, and I. W. Levin, Appl. Spectrosc. **51,** 563 (1997).
4. L. H. Kidder, I. W. Levin, E. N. Lewis, V. D. Kleiman, and E. J. Heilweil, Opt. Lett. **22,** 742 (1997).
5. R. Bhargava, M. D. Schaeberle, D. C. Fernandez, and I. W. Levin, Appl. Spectrosc. **55,** 1079 (2001).
6. R. Bhargava and I. W. Levin, Appl. Spectrosc. **57,** 357 (2003).
7. C. Marcott, R. C. Reeder, J. A. Sweat, D. D. Panzer, and D. L. Wetzel, Vib. Spectrosc. **19,** 123 (1999).
8. R. Mendelsohn, M. E. Rerek, and D. J. Moore, Phys. Chem. Chem. Phys. **2,** 4651 (2000).
9. P. Lasch, M. Boese, A. Pacifico, and M. Diem, Vib. Spectrosc. **28,** 147 (2002).
10. B. O. Budevska, S. T. Sum, and T. J. Jones, Appl. Spectrosc. **57,** 124 (2003).
11. P. Garidel, Phys. Chem. Chem. Phys. **5,** 2673 (2003).
12. C. M. Snively and J. L. Koenig, Macromolecules **31,** 3753 (1998).
13. C. M. Snively and J. L. Koenig, J. Polym. Sci. B, Polym. Phys. **37,** 2353 (1999).
14. G. Y. Li and J. L. Koenig, Appl. Spectrosc. **56,** 1390 (2002).
15. J. M. Chalmers, N. J. Everall, M. D. Schaeberle, I. W. Levin, E. N. Lewis, L. H. Kidder, J. Wilson, and R. Crocombe, Vib. Spectrosc. **30,** 43 (2002).
16. S. J. Oh, J. S. Do, and J. H. Ok, Appl. Spectrosc. **57,** 1058 (2003).
17. S. G. Kazarian and K. L. A. Chan, Macromolecules **37,** 579 (2004).
18. H. H. Richardson, V. W. Pabst, and J. A. Butcher, Appl. Spectrosc. **44,** 822 (1990).
19. S. M. Alawi, T. Krung, and H. H. Richardson, Appl. Spectrosc. **47,** 1626 (1993).
20. P. Hamm, S. Wiemmann, M. Zurek, and W. Zinth, Opt. Lett. **19,** 1642 (1994).
21. S. M. Arrivo, V. D. Kleiman, T. P. Dougherty, and E. J. Heilweil, Opt. Lett. **22,** 1488 (1997).
22. D. L. Elmore, M.-W. Tsao, S. Frisk, D. B. Chase, and J. F. Rabolt, Appl. Spectrosc. **56,** 145 (2002).
23. C. Pellerin, C. M. Snively, D. B. Chase, and J. F. Rabolt, Appl. Spectrosc. **58,** 639 (2004).
24. J. Zhao, Appl. Spectrosc. **57,** 1368 (2003).
25. J. Zhao and F. S. Allen, U.S. Patent 66,636,305 (2003).
26. W. G. Fastie and O. Mills, U.S. Patent 2,757,568 (1956).
27. W. G. Fastie, O. Mills, and W. M. Sinton, U.S. Patent 2,922,331 (1960).
28. V. L. Chupp, U.S. Patent 3,939,191 (1976).
29. M. P. Chrisp, U.S. Patent 5,880,834 (1999).
30. F. Blechinger, U.S. Patent 4,773,756 (1988).
31. S. Krimm, Adv. Polym. Sci. **2,** 51 (1960).